Int. J. Electrochem. Sci., 12 **(2017)** 3941 – 3949, doi: 10.20964/2017.05.65

International Journal of
ELECTROCHEMICAL
SCIENCE
www.electrochemsci.org

One-pot Synthesis of Cuprous Oxide-Reduced Graphene Oxide Nanocomposite as an Anode Material for Lithium Ion Battery

Yi Lu[1,2,*], *Tao Wang*[2], *Zhaojun Tian*[2] *and Qing Ye*[2]

[1] Hunan University of Science and Technology, Work Safety Key Lab on Prevention and Control of Gas and Roof Disasters for Southern Coal Mines, Xiangtan, Hunan 411201, China
[2] Hunan University of Science and Technology, School of Resource, Environment and Safety Engineering, Xiangtan, Hunan 411201, China
[*]E-mail: luyihnust@163.com

Received: 23 February 2017 / *Accepted:* 4 April 2017 / *Published:* 12 April 2017

With the simultaneous reduction of Cu^{2+} ions and GO by ethylene glycol, this work explores the convenient and one-pot preparation of porous cuprous oxide nanoparticles on reduced graphene oxide (Cu_2O–RGO). A series of measurements were applied for the characterization of the surface morphology, crystal structure and basic chemical elements of synthesized nanocomposite. An increase of initial discharge capacity to 2038 mAh/g was observed for the battery due to the synergetic effect of wrinkled graphene & copper oxide. This study conducts the impedance spectroscopy for obtaining charge transfer resistance of the electrode, with the results analysed herein.

Keywords: One-pot; Graphene; Cuprous oxide; Lithium ions; Battery

1. INTRODUCTION

Featuring conversion reaction, the electrodes based on metal oxides are endowed with elevated specific capacity, thus the role of metal oxides as electrode materials has gone through diverse investigation for lithium ion batteries. What impedes the actual use of such electrodes is attributed to poor cycle stability to the cell caused by their expansion in volume, where the investigation is conducted for transition metal oxides including Cu_2O, CuO, Co_3O_4, Mn_3O_4, Fe_2O_3 and so on [1-7]. The behaviour of battery is also significantly influenced by the morphs of such oxides [8]. The capacity maintenance is achieved mainly by controlled synthesis of these materials. The metal oxides can also be employed in synthesizing structures of metal oxide carbon nanotube hybrid and metal oxide graphene hybrid [9-12]. Despite the restricted specific capacity (374 mAh/g) of Cu_2O, researchers have

been interested in its practical use in the field of lithium ion battery. The electrochemical behaviour of Cu_2O anode with diverse crystal planes was issued by Chen and co-workers, with elevated electroactivities of Cu_2O facets to redox reaction [13].

The distinctive electrochemical and physical traits enable graphene (a new carbon derivative) to be appealing to more and more researchers. Safety, convenient procedure, high surface area and other possible merits would be indicated in the application of graphene as a modifier in electrochemical aspect [14]. In addition, graphene performs excellently in electrical conductance (64 mS/cm) and is endowed with extended theoretical surface area (2630 m^2/g) [15, 16], together with high electron shift rate, low charge-shift resistance and large potential window. It has been reported that the anode samples for lithium ion battery can be prepared with numbers of polymer coated graphene and metal oxide decorated graphene [17-22]. The restacking issue still exists for few layer graphene. It has not been figured out how to fully utilize the top & bottom layers of the 2D structure. Literatures reveal that the problem of restacking can be solved during the fabrication of graphene-CNT hybrid structure, while carbon nanotube has a restricted function of offering lithium ions a short diffusion path length as a spacer. Therefore in terms of the specific capacitance of the battery, it is essential for a material with the function of both contributor and spacer to be explored.

Through a facile one-pot solvothermal approach, this work efficiently studies the loading of the Cu_2O nanoparticles on RGO. Cu_2O features consistent nanoparticles diameter. Meanwhile the favorable dispersion of the nanoparticles can be observed on the 2D graphene sheets. A range of methods were employed for the characterization of as-synthesized Cu_2O/RGO nanocomposites. In terms of specific capacitance of the battery, the investigation of Cu_2O used as its conversion electrode contributor and spacer is herein conducted.

2. EXPERIMENTS

With the natural graphite employed as precursor, the synthesis of GO was conducted via designed Hummers approach [23]. To be brief, after the addition of $NaNO_3$ (1.25 g) and graphite powder (2 g) to concentrated H_2SO_4 (60 mL), cooling and stirring were conducted to keep the mixture below 20 °C during the gradual addition of $KMnO_4$ (7.5 g), followed by 0.5 h stirring at 35 °C. Subsequently the mixture was gradually infused with distilled water (120 mL), with a rise of temperature to 98 °C which stayed for 15 min. Then the reaction was finished after the successive infusion of distilled water (350 mL) and H_2O_2 solution (10 mL, 30%). The centrifugation separation and repeated HCl solution (5%) washing were conducted for the solid product till the sulfate was undetectable by $BaCl_2$. Subsequently it went through triple ethanol washing and 60 °C vacuum drying overnight.

With the addition of GO, the copper(II) acetate was chemically reduced in ethylene glycol solution, thus fabricating the Cu_2O-RGO nanocomposites. A characteristic synthesis process featured the dispersion of copper(II) acetate monohydrate (100 mg) and GO (50 mg) in EG (50 mL), with the infusion of as-prepared mixture to a steel autoclave (100 mL). After the sealing, this container kept a temperature of 180 °C for 2 h, with a subsequent ambient temperature reached through natural cooling.

The removal of the residual soluble byproducts and ethylene glycol was achieved through repeated filtration and ample ethanol washing of as-prepared mixture. Subsequently, with its drying conducted in a vacuum desiccator, the final product, Cu_2O-RGO was synthesized. To make comparisons, the same process was employed to generate RGO and Cu_2O specimens.

On a TD-3500X X-ray diffractometer featuring Cu Ka radiation, X-ray powder diffraction (XRD) was conducted for the evaluation of the crystal structure of as-prepared specimens. Standard 2032-type coin cells provided platforms for testing the electrochemical traits of these specimens. The homogeneous slurry generated through the dispersion of polyvinylidene fluoride (PVDF) (10 wt%), acetylene black (10 wt%) and active materials (80 wt%) into N-methyl-2-pyrrolidone (NMP) contributed to the preparation of the working electrodes. Then after the uniform coating on the Cu foil, the as-prepared slurry went through vacuum drying for 8 h at the temperature of 120 °C. The combination of ethylene carbonate (EC) & dimethyl carbonate (DMC) (1:1 v/v) and $LiPF_6$ (1 M) contributed to the electrolyte, while the role of reference electrode and counter electrode were taken by the lithium foil. The concentrations of both the moisture and oxygen were kept below 1ppm in the Ar-filled glove box where the assembling of cells was conducted. With a voltage ranging from 0 to 3 V and a 100 mA g-1 current density, the charge/discharge were measured at ambient temperature via Battery Testing System (Neware BTS-610). A CHI760E electrochemical workstation provided the platform for experiments concerning electrochemical impedance spectroscopy (EIS) and cyclic voltammetry (CV) carried out at ambient temperature. Herein EIS measurements were conducted with a amplitude of 5 mV and a frequency ranging from 0.1 to 10000 Hz, and the CV measurements carried out with 0.2 mV/s as its scan rate.

3. RESULTS AND DISCUSSION

The as-prepared Cu_2O/RGO nanocomposite had its morphology characterized through SEM. The successful synthesis of the Cu_2O/RGO nanocomposite is obviously observed in Figure 1A. The corrugation is exhibited for the sheets of RGO. The effective prevention of RGO sheets stacking is realized through the decoration of Cu_2O nanoparticles on two sides of the sheet. The nanoparticle of Cu_2O with an average size of 40 nm was generated through galvanic displacement. Base on the observation, graphene can prevent the continuous growth of the spheres and at the same time avoid intensive aggregation of the nanoparticles [24]. For composite formation, specifically, Cu_2O tends to nucleate on the GO surface in the beginning of the reaction due to the abundance of functional groups on the GO sheets. Subsequently, Cu nanoparticles are gradually produced by the redox etching of the outside of the Cu_2O nanospheres with the extension of the reaction time [25].

Figure 1B reveals the crystal data for Cu_2O/RGO nanocomposite and GO, where a distinctive diffraction peak (002) can be observed via XRD at roughly 10° for GO. This peak denotes a d-spacing of 0.772 nm, while the (002) peak for graphite indicates a much smaller interlayer distance. The contrast may lie in the attachment of carbonyl (–C=O) groups, carboxyl (–COOH), hydroxyl (–OH), epoxy and other oxygenated functional species on two edges and sides of the carbon sheets. Cu_2O (JCPDS 78-2076) has its (311), (220), (200), (111) and (110) crystal planes revealed through

corresponding diffraction peaks for Cu_2O/RGO nanocomposite, as shown in XRD profile. No diffraction peaks for graphene can be observed because of the low quantity and relatively low intensity of graphene in the sample [26]. In addition, the desirable crystallization and purity of as-synthesized nanocomposites are revealed through the absence of impurities peaks.

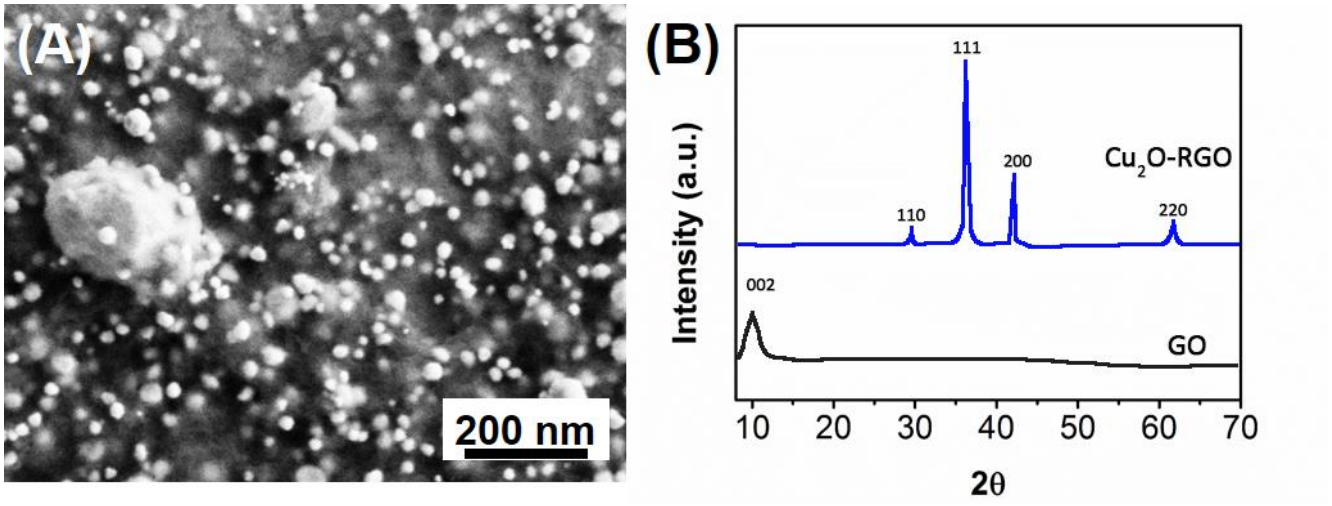

Figure 1. (A) SEM image and (B) XRD pattern of Cu_2O/RGO nanocomposite.

Cu_2O-RGO nanocomposite is characterized via Raman spectrum in Figure 2A. Cu_2O vibration modes of$\Gamma_{12}^{-(2)}$, $4\Gamma_{12}^{-}$ and $2\Gamma_{12}^{-}$ respectively correspond to 624, 401 and 218 cm^{-1}Raman bands [27]. The diamondoid (D band, breathing mode of κ-point photons of A_{1g} symmetry) band was located at 1335 cm^{-1}, while the graphite (G band, first-order scattering of E_{2g} phonons by sp^2 carbon atoms) band at 1572 cm^{-1} [28]. 2707 cm^{-1} is observed to be the 2-D peak for Cu_2O-RGO nanocomposites. As the layers increase in number in terms of single-layer graphene (2-D, 2680 cm^{-1}), the peak transfers to more elevated wave number value and turns wider. The D band at 1310 cm^{-1} becomes prominent due to the reduction in the size of plane sp^2 domains, possibly as a result of extensive oxidation [29]. Two phonons with diverse momentum are combined together, thus leading to defects, which are suggested through the 2938 cm^{-1} (D+D′) peak [30]. The statistics herein indicate that the Cu_2O-RGO composites have been formed.

GO and Cu_2O/RGO nanocomposite are characterized through FTIR spectra in Figure 2B. A string of species containing oxygen were indicated in GO, where the C=O vibration of —COOH positioned at edge of GO sheets is revealed through the 1722 cm^{-1} band and the stretching vibration of O—H explains the significant band at roughly 3397 cm^{-1}. Besides, the stretching vibration of tertiary C—OH species is reflected by the 1392 cm^{-1} peak, while the characteristics of O—H, epoxide groups and skeletal bending vibration are observable at 1618 cm^{-1}. Meanwhile, C—O stretching vibrations contribute to the 1050 cm^{-1} and 1225 cm^{-1} band. As for Cu_2O/RGO nanocomposite, it can be seen that Cu—O bonds are perturbed as RGO interacts with Cu_2O, as revealed from the 622 cm^{-1} band for Cu—O vibration of Cu_2O. The efficient GO reduction is suggested by the skeletal vibration of C=C of

the RGO sheets, corresponding to the 1587 cm^{-1} band. The peaks centered at 615 cm^{-1} are associated with Cu_2O, verifying the results of XRD measurements [31].

The data of Li-ion insertion-extraction concerning electrochemical reactions were obtained via CV. The original Cu_2O and Cu_2O/RGO composite are respectively characterized through the top three CV curves in Figure 3. The reduction of Cu_2O to Cu is revealed by the cathodic peak at 1.33 V, the formation of solid electrolyte interface (SEI) layer by the cathodic peak at 0.84 V, and the lithium insertion to the Cu2O by the cathodic peak at 0.51 V. These peaks in terms of Cu_2O specimen are observed in through the cathodic scan for the first round.

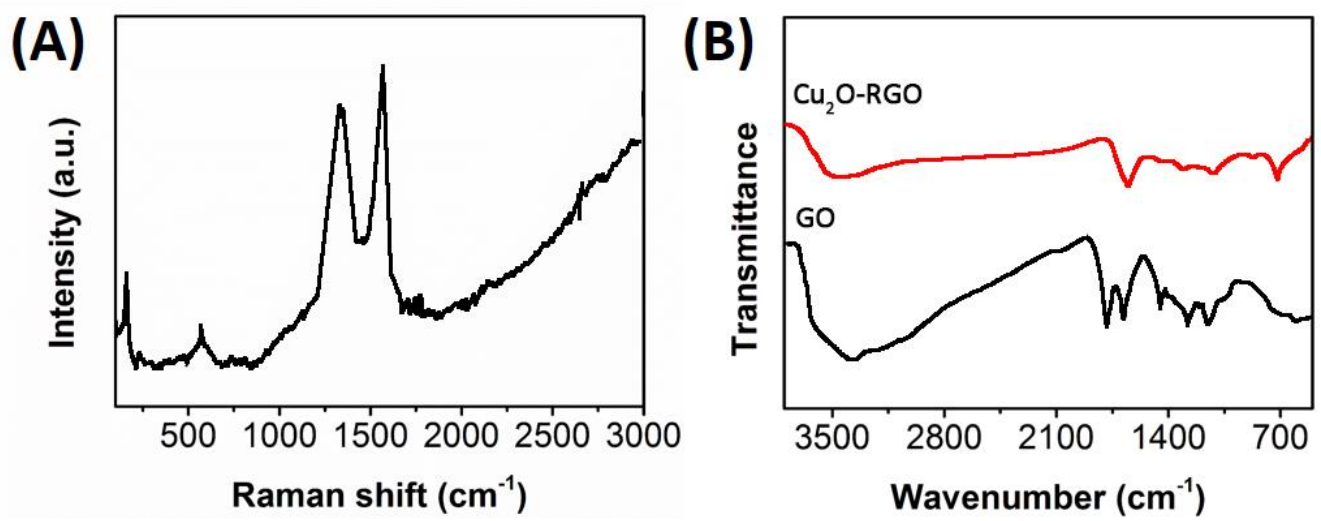

Figure 2. (A) Raman spectra and (B) FTIR spectra of GO and Cu_2O/RGO nanocomposite.

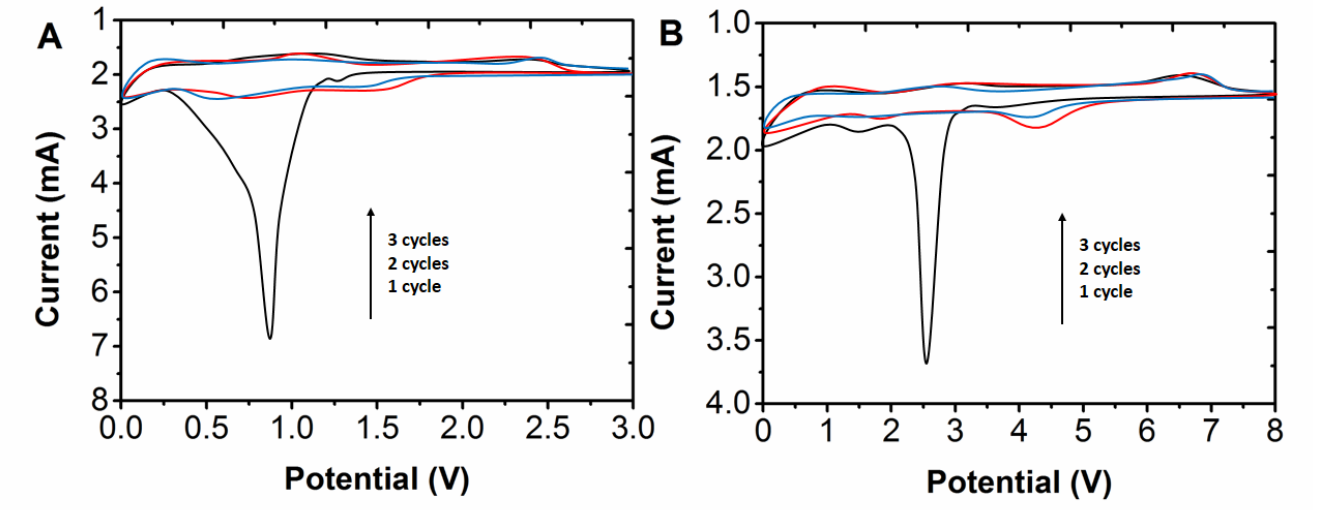

Figure 3. CV of (A) pure Cu_2O, (B) Cu_2O/RGO electrodes between 0 and 3.0 V at a scan rate of 0.2 mV/s for the first three cycles.

Through subsequent scans, the 0.87 V cathodic peak was unobservable again. In addition to the cathodic peaks, anodic peaks are also detected. The oxidization of Cu to Cu_2O is reflected through the

2.38 V and 0.95 V anodic peaks. Roughly 1.33/2.38 V and 0.51/0.95 V for two cathodic/anodic couples could be detected in the following cycles. Better performance of the electrode in reversibility was revealed through the steady curves. The Cu_2O specimen shares similarities with Cu_2O/RGO composite in CV curves through their comparison. However, the peaks of the latter one transferred, together with narrowed separation (ΔE) and a decline in intensities between the redox couples. Because of the low graphene content, only peaks concerning the graphene are observed in terms of Cu_2O/RGO composite.

The electrochemical behavior of the cell was indicated through the investigation of Cu_2O/RGO electrode with theinsertion-extraction of lithium. At ambient temperature, the testing of the assembled cell was carried out in the voltage window of 0.01 V and 3 V. Cu_2O/RGO is characterized through charge-discharge curve in Figure 4, where 2038 mAh/g is obtained for the initial discharge capacity. The SEI layer is formed on the surface of the anode, as reflected through a steady capacity in other six cycles herein. On the basis of the electrode reaction, the theoretical Cu_2O capacity (355 mAh/g) is relatively lower than that of the electrode. Despite the significant difference between the specific capacity of the electrode and the conversion-reaction-based prediction in theory, this is a conversion reaction carried out on the surface of electrode. The solid electrolyte interface is formed on the electrode surface, thus leading to the significant initial capacity. Herein the formation of Li_2O and Cu[0] is achieved through the interaction between the copper oxide and lithium ion, where the re-oxidisation back to +2 state from the zero oxidation state for most of the copper would not occur. The SEI layer is made up of ethylene oxide based oligomers, LiF, $LiCO_3$ and lithium alkyl carbonate that controls the exertion and insertion of lithium ion via the electrode, which is characterised through the charge–discharge curve of the electrode.

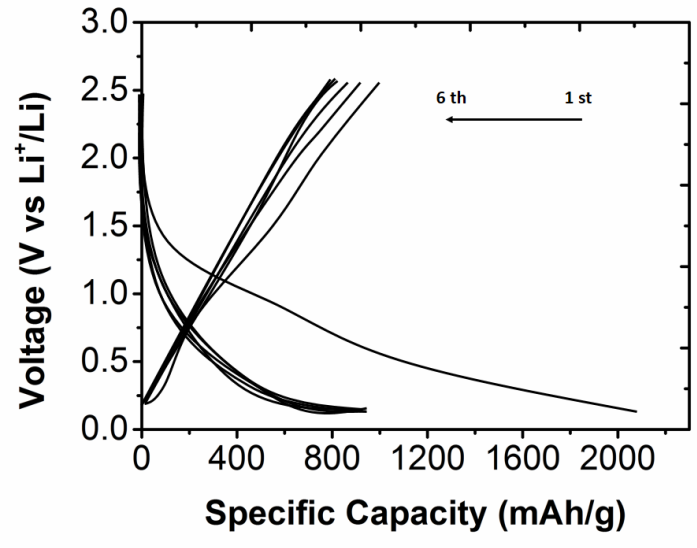

Figure 4. Galvanostatic charge–discharge profile for Cu_2O/RGO in the voltage range 0.01–3 V vs. Li/Li^+ electrode.

The charge-discharge profile is detected to be steady after the first cycle, since it functions as a passivation layer. With a favourable performance in connectivity to copper oxide beads and electronic conductivity, the graphene featuring awrinkled property prevents the electrode to be polarized. The Cu_2O/RGO material herein can be seen as a new type of specially structured composite with theoretical capacity larger than pure Cu_2O. Its high capacity and superior cycling performance again highlight the crucial role of RGO in alleviating the capacity degradation and at the same time show a surprising synergetic effect of the dual-conducting system.

The discharge-charge mode was employed to measure the whole set of specimens between 0 and 3 V at a current density of 100 mA/g, in order to further explore the influence of nanostructure exerted on the cycling behavior. Figure 5 exhibits the coulombic efficiency and cycle curves of the specimens. In the first cycle, there is a significant decline for the discharge capacity of the whole set of specimens. However, with roughly 99 % coulombic efficiency, the steady discharge and charge capacity is observable since the 5th cycle. In the initial cycle, the discharge capacities of 472 mAh/g are delivered by Cu_2O. And after 50 cycles, Cu_2O delivers the discharge capacities of 125 mAh/g. on the other hand, the discharge capacity of 730 mAh/g are delivered by Cu_2O/RGO composite in the initial cycle, while remaining 371 mAh/g after 50 cycles. In comparison, the previously issued 348.4 mAh/g is much lower. The relief of the volume contraction/expansion and the enhancement of Cu_2O conductivity can be achieved by RGO, as revealed herein. The comparison of the Cu_2O/RGO anode with other recent anode materials were listed in the Table1. It can be seen that our proposed Cu_2O/RGO exhibited a fair performance.

,

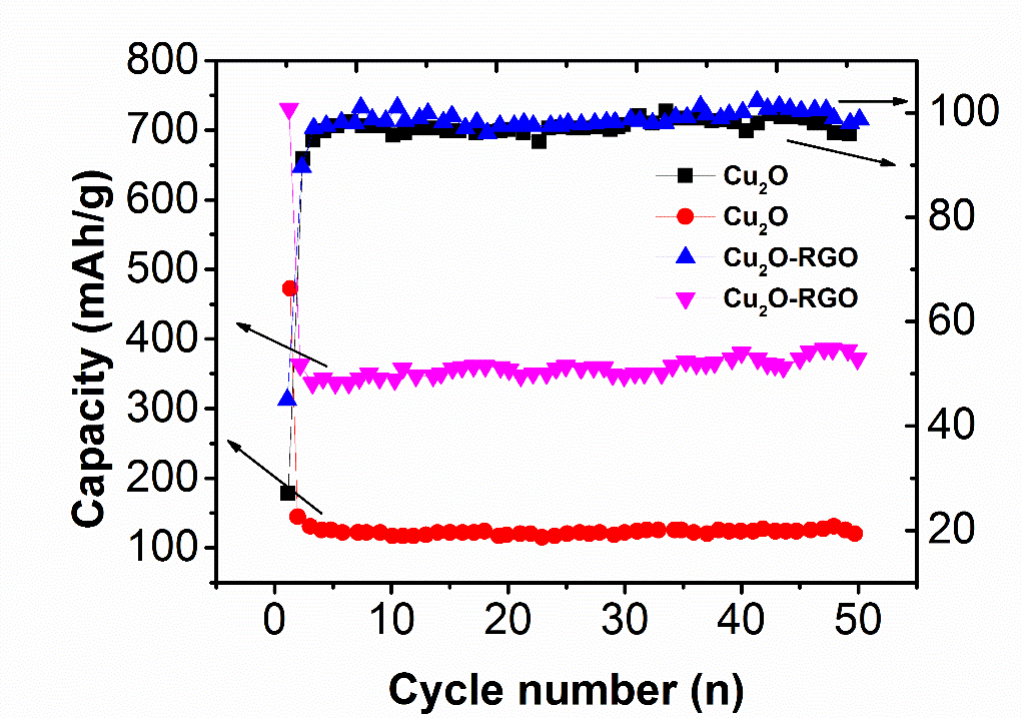

Figure 5. Comparative cycling performance and coulombic efficiency of pure Cu_2O and Cu_2O/RGO electrodes at the current density of 100 mA/g.

Table 1. The capacity of Cu_2O/RGO with some composites in recent years.

Composite	Specific capacity (mAh/g)	Cycle No.	Reference
SnSb-ZnO	751	100	44
SnO_2/ZnO	430.6	100	[32]
SnO_2/ZnO	450	50	[33]
SnO_2/ZnO	521.1	80	[34]
SnO-ZnO/graphene	800	50	[35]
Cu_2O/RGO	730	50	This work

EIS was employed after cycling at OCP of 0.9 V with a frequency ranging from 0.1 Hz to 100 KHz, apart from its engagement in the investigation of the cell charge shift resistance. An equivalent circuit corresponds to the experimental data. There are also two resistances-constant phase element parallel circuits corresponding to the data. Herein the formation of the SEI layer resistance on the electrode surface is indicated by the initial R–CPE combination, while the electrode charge–shift resistance is manifested through the following R-CPE. The charge shift resistance and SEI layer resistance are respected represented by 21 Ω and 32 Ω, as revealed through the fitted data. In comparison with previous graphene and graphene composite electrodes based literature, charge shift resistance of the electrode is relatively low [36, 37]. Herein the synergetic effect of Cu_2O-graphene composite is emphasized.

4. CONCLUSIONS

To conclude, a facile one-pot hydrothermal method enables the synthesis of Cu_2O-RGO nanocomposite to be conducted and also realizes a simultaneous fabrication of RGO sheets and Cu_2O nanoparticles in this study. An increase of the initial discharge capacity of the battery to 2038 mAh/g and 472 mAh/g for 25 cycles with columbic efficiency of 99% is observed due to the synergetic effect of wrinkled graphene and copper oxide. The double functions of Cu_2O used as a conversion electrode contributor and a spacer were herein reported.

ACKNOWLEDGEMENTS
This work was supported by the National Natural Science Foundation of China (51604110, 51274100, U1361118, 51504093 and 51374003) and Scientific Research Foundation for Doctor of Hunan University of Science and Technology (E51650).

References

1. L. Hu, Y. Huang, F. Zhang and Q. Chen, *Nanoscale*, 5 (2013) 4186.
2. M. Reddy, T. Yu, C. Sow, Z. Shen, C. Lim, G. Subba Rao and B. Chowdari, *Adv Funct Mater*, 17 (2010) 2792.
3. J. Gao, M. Lowe and H. Abruña, *Chemistry of Materials*, 23 (2011) 3223.
4. Y. Yao, J. Zhang, T. Huang, H. Mao and A. Yu, *Int. J. Electrochem. Sc.*, 8 (2013) 3302.
5. N. Yan, L. Hu, Y. Li, Y. Wang, H. Zhong, X. Hu, X. Kong and Q. Chen, *Journal of Physical Chemistry C*, 116 (2012) 7227.
6. R. Sahay, P.S. Kumar, V. Aravindan, J. Sundaramurthy, W. Ling, S. Mhaisalkar, S. Ramakrishna

and S. Madhavi, *Journal of Physical Chemistry C*, 116 (2012) 18087.
7. C. Ji, J. Kim, H. Kwon and H. Song, *Adv. Mater.*, 40 (2009) 803.
8. C. Wang, Q. Li, F. Wang, G. Xia, R. Liu, D. Li, N. Li, J. Spendelow and G. Wu, *ACS Applied Materials & Interfaces*, 6 (2014) 1243.
9. Y. Mai, X. Wang, J. Xiang, Y. Qiao, D. Zhang, C. Gu and J. Tu, *Electrochimica Acta*, 56 (2011) 2306.
10. Y. Xu, Y. Guo, C. Li, X. Zhou, M. Tucker, X. Fu, R. Sun and C. Wong, *Nano Energy*, 11 (2015) 38.
11. S. Choi, J. Lee and Y. Kang, *Acs Nano*, 9 (2015) 10173.
12. S. Yu, X. Guo, D. Ling, Y. Dong, A. Jin, M. Shokouhimehr, T. Hyeon and Y. Sung, *Rsc Advances*, 4 (2014) 37365.
13. K. Chen, S. Song and D. Xue, *Crystengcomm*, 17 (2015) 2110.
14. S. Wu, Q. He, C. Tan, Y. Wang and H. Zhang, *Small*, 9 (2013) 1160.
15. M. Stoller, S. Park, Y. Zhu, J. An and R. Ruoff, *Nano Letters*, 8 (2008) 3498.
16. C. Liu, S. Alwarappan, Z. Chen, X. Kong and C. Li, *Biosensors and Bioelectronics*, 25 (2010) 1829.
17. F. Ye, B. Zhao, R. Ran and Z. Shao, *Journal of Power Sources*, 290 (2015) 61.
18. Z. Li, H. Zhang, Q. Liu, Y. Liu, L. Stanciu and J. Xie, *ACS Applied Materials & Interfaces*, 6 (2014) 5996.
19. L. Mei, J. Feng, L. Wu, J. Chen, L. Shen, Y. Xie and A. Wang, *Microchim. Acta.*, 183 (2016) 2039.
20. Y. Zheng, Z. Wang, F. Peng, A. Wang, X. Cai and L. Fu, *Fullerenes, Nanotubes and Carbon Nanostructures*, 24 (2016) 149.
21. M. Velmurugan, N. Karikalan, S. Chen and C. Karuppiah, *Microchim. Acta.*, 183 (2016) 2713.
22. X. Liu and J. Sun, *Nano*, 11 (2016) 1650102.
23. W. Hummers and R. Offeman, *Journal of the American Chemical Society*, 80 (1958) 1339.
24. N. Li, Y. Xiao, C. Hu and M. Cao, *Chemistry–An Asian Journal*, 8 (2013) 1960.
25. M. Elahi, A. Khodadadi and Y. Mortazavi, *Journal of The Electrochemical Society*, 161 (2014) B81.
26. A. Dubale, W. Su, A. Tamirat, C. Pan, B. Aragaw, H. Chen, C.. Chen and B. Hwang, *Journal of Materials Chemistry A*, 2 (2014) 18383.
27. S. Deng, V. Tjoa, H. Fan, H. Tan, D. Sayle, M. Olivo, S. Mhaisalkar, J. Wei and C. Sow, *Journal of the American Chemical Society*, 134 (2012) 4905.
28. Z. Fan, W. Kai, J. Yan, T. Wei, L. Zhi, J. Feng, Y. Ren, L. Song and F. Wei, *ACS Nano*, 5 (2010) 191.
29. C. Chen, T. Chen, H. Wang, G. Sun and X. Yang, *Nanotechnology*, 22 (2011) 405602.
30. D. Elias, R. Nair, T. Mohiuddin, S. Morozov, P. Blake, M. Halsall, A. Ferrari, D. Boukhvalov, M. Katsnelson and A. Geim, *Science*, 323 (2009) 610.
31. G. Papadimitropoulos, N. Vourdas, V.E. Vamvakas and D. Davazoglou, *Thin Solid Films*, 515 (2006) 2428.
32. Y. Zhao, X. Li, L. Dong, B. Yan, H. Shan, D. Li and X. Sun, *International Journal of Hydrogen Energy*, 40 (2015) 14338.
33. Y. Huang, X. Liu, L. Lu, J. Fang, H. Ni and Z. Ji, *Applied Physics A*, 120 (2015) 519.
34. J. Zhu, G. Zhang, S. Gu and B. Lu, *Electrochimica Acta*, 150 (2014) 308.
35. Q. Guo, S. Chen and X. Qin, *Mater. Lett.*, 128 (2014) 50.
36. P. Nayak and S. Ramaprabhu, *Journal of Physical Chemistry C*, 119 (2015) 2917-2924.
37. G. Yan, L. Xin-Hai, Z. Wang, H. Guo, Q. Zhang and W. Peng, *Zhongguo Jingshu Xuebao*, 23 (2013) 3691.